SPACECRAFT RELATIVE MOTION WITH RESPECT TO A SPINNING CHIEF BODY FRAME

Afrah Ghedira[*] and Hanspeter Schaub[†]

Relative motion between orbiting spacecraft is often modeled in the Hill frame due to its analytical first-order solutions and the intuitive geometry of the resulting orbits. However, this frame is not ideal for mission scenarios involving constraints fixed in the body frame, such as collision avoidance when approaching and docking onto spinning objects. This paper studies analytical solutions for relative motion in the body frame for a circular chief orbit and derives geometrically meaningful invariants that provide intuitive insight into the resulting relative trajectory shapes. Both bounded and drifting motions are considered. Further, the body frames are initially aligned with the Hill frame and undergoing constant rotation about each Hill frame principal axis (radial, along-track, and cross-track). The analysis includes both resonant (spin rate equal to the orbital rate) and non-resonant cases.

INTRODUCTION

Orbital rendezvous and docking technologies date back to the early days of the space race. These pioneering rendezvous approaches initially relied heavily on human guidance.[1] Historically, most on-orbit servicing and assembly, such as operations on the International Space Station (ISS) or the Hubble Space Telescope, have also required direct human control.[2]

More recently, the focus has shifted toward fully autonomous robotic rendezvous and docking, driven by the increasing demand for these capabilities and the risks associated with operations. This shift is fueled by growing interest in applications such as active debris removal, on-orbit servicing and assembly, and satellite life extension through upgrades and refueling.[3,4] Several space missions have been developed as technology demonstrations of autonomous rendezvous and docking technologies. For example, the Orbital Express (OE) project,[5] supported by the Defense Advanced Research Projects Agency (DARPA), demonstrated autonomous rendezvous that involved battery and CPU module exchange, as well as propellant transfer. This was carried out between two controlled spacecraft: the ASTRO servicing satellite and a prototype modular client[*]. Commercial interest is also growing for autonomous rendezvous technologies. For instance, Astroscale's Life Extension In-orbit (LEXI) Servicer, scheduled to launch to GEO by 2026, aims to provide life-extension services for commercial satellites.[†] Additionally, Astroscale demonstrated autonomous

[*]Graduate Research Assistant, Ann and H.J. Smead Department of Aerospace Engineering Sciences, University of Colorado Boulder, Colorado Center for Astrodynamics Research, Boulder, CO, 80303 USA. afrah.ghedira@colorado.edu

[†]Distinguished Professor and Department Chair, Schaden Leadership Chair, Ann and H.J. Smead Department of Aerospace Engineering Sciences, University of Colorado Boulder, Colorado Center for Astrodynamics Research, Boulder, CO, 80303 USA. AAS Fellow, AIAA Fellow

[*]https://ai.jpl.nasa.gov/public/projects/orbital-express/

[†]https://astroscale-us.com/lexi-life-extension-capabilities/

rendezvous with an uncontrolled object during the ELSA-d mission, using a servicer-client pair designed to simulate debris removal scenarios.[6]

GEO remains a prime target for servicing missions, as it hosts some of the largest and most valuable satellite assets, making it a region of both commercial and national strategic interest.[4] With this evolving focus, technological challenges are becoming more complex. These include the need to rendezvous with uncooperative targets, objects that may be spinning or tumbling due to malfunctions or by design. In some missions, spinning is deliberately introduced, such as in dual-spinner configurations, or to maintain instrument pointing.[7] Some satellites stabilize the attitude using spin stabilization about a major principal axes. Other satellites have mission requirements that lead it to rotate continuously using a modern three-axis attitude control system.[8,9] These dynamic conditions significantly complicate final approach and docking maneuvers, particularly in the presence of collision avoidance ("keep-out") or docking ("keep-in") zones. As a result, rendezvous with spinning or tumbling targets has emerged as an active area of research. Numerous studies are focused on developing guidance, motion planning algorithms, and control techniques to ensure safe and reliable approach and docking.[10–15]

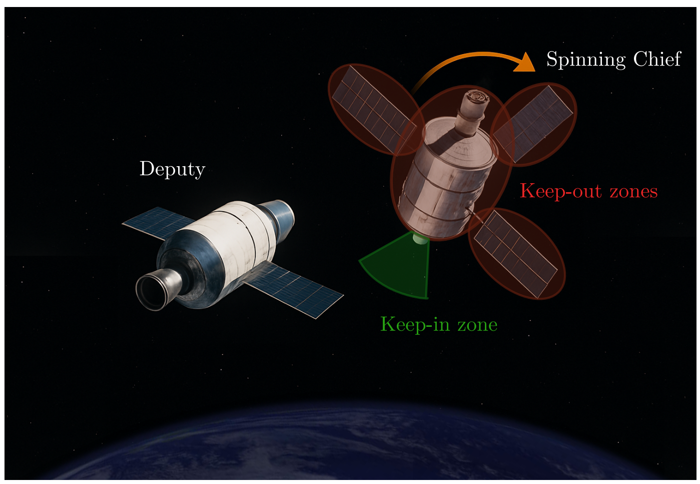

Figure 1. Concept figure of a servicing mission to a spinning chief.

In Rendezvous and Proximity Operations (RPO) missions, the relative motion of the chaser, or "deputy", is commonly modeled using the Hill frame, a rotating coordinate system centered on the target spacecraft, or "chief".[16] This representation offers a variety of analytical solutions that efficiently describe relative trajectories without requiring computationally intensive numerical integration. As such, it is well-suited for both onboard Guidance, Navigation, and Control (GNC) systems and offline mission planning.[17] A widely used example is the Clohessy–Wiltshire (CW) equations,[18] which describe the deputy's translational motion in Cartesian coordinates. These closed-form solutions define relative motion using six Relative Orbital Elements (ROEs), or invariants of motion, derived from the initial conditions.[19] The ROEs describe the size, shape, and orientation of the relative orbit, yielding intuitive trajectory representations. Alternatively, some methods represent the deputy's state using combinations of the absolute orbital elements of both the chief and deputy.[20,21] However, when dealing with spinning or tumbling targets, the Hill frame becomes less practical during the final approach. In such scenarios, mission-critical constraints like sensor keep-in zones for docking or structural keep-out zones are often best represented in the target's body-fixed frame.

While previous studies, such as 10, have proposed motion planning techniques for rendezvous with rotating targets, they typically do not model the full relative dynamics within the target's rotating frame. As a result, the target's rotation is often incorporated through time-varying constraints, adding complexity to the planning problem. This motivates the objective of the present work: to directly model and analyze the relative motion of a deputy spacecraft from the perspective of a spinning chief, using the chief's own rotating body-fixed frame as the reference.

Reference 22 derives first-order analytical solutions for relative motion in a chief-centered inertial frame using Inertial-frame Relative Orbit Elements (IROE), which are based on parameters of an epitrochoid curve. This formulation is particularly advantageous for mission design scenarios with constraints fixed in the inertial frame, such as servicing operations involving inertially-fixed keep-in or keep-out zones impacting lighting or local space plasma conditions.[22] Notably, in the case of a controlled, non-rotating satellite, without loss of generality the inertial frame can be assumed to align with the body-fixed frame, making the insights directly applicable in that context. This paper extends the work in Reference 22 by analyzing the case of a spinning target spacecraft, where the target's body-fixed frame and the inertial frame are no longer aligned. The objective, therefore, is to examine the deputy's relative motion as observed from the chief's rotating body frame and to introduce a new formulation featuring geometrically meaningful invariants of motion. The derivations assume an initial alignment between the target's body-fixed frame and the Hill frame, while accounting for constant angular rotation about each of the principal axes. Both resonant (where the spin rate equals the orbital rate) and non-resonant scenarios are considered. The resulting analysis captures both bounded and drifting relative motion, offering deeper insight into the deputy's trajectory as observed from the spinning body frame under these specific spin conditions.

The paper begins with a problem statement that outlines the scope of the study, provides the background, and defines the reference frames used throughout the analysis. The following section introduces the general linearized solution, detailing the methodology for expressing the motion in the body frame and presenting representative trajectory examples. This is followed by three dedicated sections, one for each spin configuration (orbit-normal, nadir-pointing, and along-track), which explore each case in detail, analyze specific scenarios, and discuss the resulting body-frame trajectories. The paper concludes with a summary of the key findings and a discussion of their implications.

PROBLEM STATEMENT

Given the inertial position and velocity vectors of the chief ($\boldsymbol{r}_c, \dot{\boldsymbol{r}}_c$) and deputy ($\boldsymbol{r}_d, \dot{\boldsymbol{r}}_d$) satellites, the relative position $\boldsymbol{\rho}$ and relative velocity $\dot{\boldsymbol{\rho}}$ in the inertial frame are defined as:

$$\begin{aligned} \boldsymbol{\rho} &= \boldsymbol{r}_d - \boldsymbol{r}_c \\ \dot{\boldsymbol{\rho}} &= \dot{\boldsymbol{r}}_d - \dot{\boldsymbol{r}}_c \end{aligned} \tag{1}$$

To describe the deputy's motion relative to the chief, the chief-centered Hill frame $\mathcal{H} = \{\hat{\boldsymbol{o}}_r, \hat{\boldsymbol{o}}_\theta, \hat{\boldsymbol{o}}_h\}$ is commonly used.[16] In this frame, $\hat{\boldsymbol{o}}_r$ is aligned with the chief's orbit radial direction, $\hat{\boldsymbol{o}}_h$ is normal to the orbit plane, and $\hat{\boldsymbol{o}}_\theta$ completes the right-handed triad in the along-track direction. These basis vectors are defined as:

$$\hat{\boldsymbol{o}}_r = \frac{\boldsymbol{r}_c}{r_c} \qquad \hat{\boldsymbol{o}}_\theta = \hat{\boldsymbol{o}}_h \times \hat{\boldsymbol{o}}_r \qquad \hat{\boldsymbol{o}}_h = \frac{\boldsymbol{r}_c \times \dot{\boldsymbol{r}}_c}{|\boldsymbol{r}_c \times \dot{\boldsymbol{r}}_c|} \tag{2}$$

Assuming the chief is in a circular orbit and that the deputy remains close (relative separation is small), the deputy's motion in the Hill frame ${}^{H}\boldsymbol{\rho} = [x, y, z]^T$ is governed by the CW equations.[18] The left superscript indicates the reference frame in which the vector is expressed:

$$\begin{aligned} \ddot{x} - 2n\dot{y} - 3n^2 x &= 0 \\ \ddot{y} + 2n\dot{x} &= 0 \\ \ddot{z} + n^2 z &= 0 \end{aligned} \tag{3}$$

where n is the mean orbit motion of the chief. The analytical closed-form solution to the CW equations is given by:[19]

$$\begin{aligned} x(t) &= A_0 \cos(nt + \alpha) + x_{\text{off}} \\ y(t) &= -2A_0 \sin(nt + \alpha) - \frac{3}{2} nt x_{\text{off}} + y_{\text{off}} \\ z(t) &= B_0 \cos(nt + \beta) \end{aligned} \tag{4}$$

This solution is characterized by six geometrically intuitive invariants of motion A_0, B_0, x_{off}, y_{off}, α and β, known as the Linearized Relative Orbit Elements (LROEs). These elements describe the shape, size, and orientation of the relative orbit. The in-plane motion traces a 2:1 ellipse, with the along-track amplitude twice the radial amplitude, governed by A_0. Offsets x_{off} and y_{off} shift the ellipse in the radial and along-track directions, respectively. An offset in the x-direction corresponds to a difference in the spacecraft orbital altitudes and therefore velocities, which causes a drift in the along-track direction. Thus, x_{off} must be zero for bounded motion. The out-of-plane motion is decoupled and corresponds to a simple harmonic oscillator, characterized by amplitude B_0. Phase angles α and β define the initial orientation of the in-plane and out-of-plane motion, respectively.

The LROEs provide an intuitive description of the relative motion in the Hill frame, which is fixed with respect to the chief's orbit. However, this frame does not account for the attitude or rotation of the spacecraft itself. Therefore, this paper investigates the relative orbit from a body-fixed frame $\mathcal{B} = \{\hat{\boldsymbol{b}}_1, \hat{\boldsymbol{b}}_2, \hat{\boldsymbol{b}}_3\}$, which is centered on the chief and aligned with its structural orientation. Figure 2 illustrates both the Hill and body frames for a spacecraft spinning, with a constant rate ω, about its radial axis, where both frames are initially aligned.

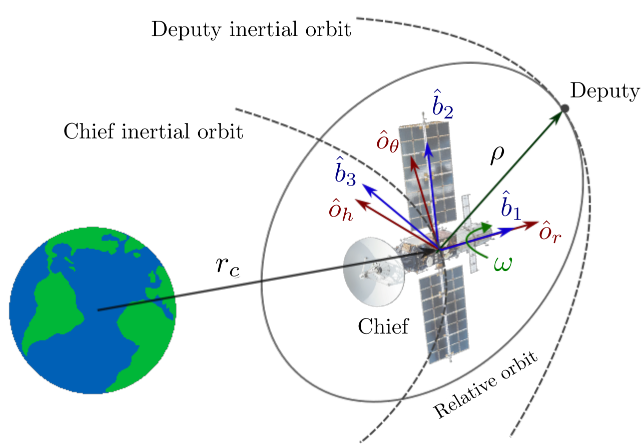

Figure 2. Illustration of the Hill frame and Body frame: Spacecraft spinning about its radial axis

Similarly to the IROEs introduced in 22, the relative motion observed in the defined body frame is analyzed and characterized using new sets of motion invariants tailored to each specific scenario. This formulation provides insight into relative dynamics for missions involving non-inertially fixed targets, such as body-referenced inspection, servicing, or docking operations.

GENERAL LINEARIZED SOLUTION

Starting from the analytical solution in Equation (3) for relative motion in the Hill frame, the corresponding motion in the body frame, denoted with the left superscript B, is obtained through a transformation using the Direction Cosine Matrix (DCM) between the two frames:

$$ {}^{B}\boldsymbol{\rho} = [BH]\ {}^{H}\boldsymbol{\rho} = [BN][HN]^{T}\ {}^{H}\boldsymbol{\rho} \tag{5} $$

where $[BH]$ denotes the DCM that transforms vectors from the Hill frame to the body frame. This matrix can be expressed as the product of $[BN]$, which maps from the inertial frame to the body frame, and $[NH] = [HN]^{T}$, which maps from the Hill frame to the inertial frame.

To compute the DCM, information about the spacecraft's attitude or spin dynamics is required. These dynamics can vary widely across mission scenarios and may include tumbling, time-varying spin rates or directions, or even completely unknown behavior, as is often the case with debris or non-cooperative targets. As a result, no single formulation can capture all possible cases. Therefore, in this study, we focus on primary spin cases, where the body frame is initially aligned with the Hill frame, and the chief spacecraft is spinning at a constant rate ω about one of its principal axes. An illustration of representative motion patterns arising from different spin and orbit configurations is provided in the figure below:

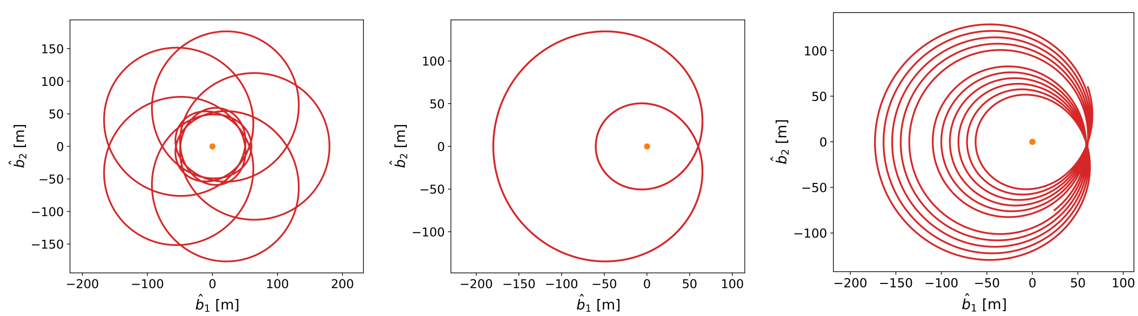

(a) Bounded motion, non-resonant spin (b) Bounded motion, resonant spin (c) Unbounded motion, resonant spin

Figure 3. In-plane trajectory shapes for an orbit-normal spin configuration.

The resulting relative trajectories resemble trochoidal curves. In particular, the motion in Figure 3(a) exhibits a hypotrochoid-like shape (generated by a point on a circle rolling inside another), while Figure 3(b) resembles an epitrochoid (generated by a point on a circle rolling outside another). Similar to the elliptical motion observed in the Hill frame, these trochoidal trajectories can also be characterized by a set of geometrically meaningful invariants. Such invariants provide a compact and intuitive way to characterize relative motion in the rotating body frame.

Note that the first two subfigures correspond to the same orbit in the Hill frame but differ in their spin configurations, non-resonant on 3(a), and resonant on 3(b). In the non-resonant case (Figure

3(a)), the trajectory shows a time-varying structure, with alternating large and small loops, indicative of time variation in their parameters. In contrast, the resonant case (Figure 3(b)) yields a simpler, closed curve. This shape is characteristic of an epitrochoid where the fixed and rolling circles have the same radius, also referred to as a Limaçon. Figure 3(c) also originates from the same nominal Hill frame trajectory, but with a change in x_{off}, meaning a difference in the semi-major axis. This induces a drift in the Hill frame motion, which manifests in the body frame as a drifting trochoidal pattern.

The following sections analyze these behaviors in more analytical detail across various spin configurations, with and without resonances, and introduce a new set of orbital elements that help characterize the motion under different orbit and spin dynamics.

ORBIT NORMAL SPIN

The first case considered in this study is a constant-rate spin about the orbit normal direction, denoted by $\hat{\boldsymbol{o}}_h$. This configuration can be observed in Earth-observing missions, where the spin helps maintain a fixed attitude relative to Earth.[7] For the scenarios examined here, the body frame is initially aligned with the Hill frame at $t = 0$, with the body's third axis $\hat{\boldsymbol{b}}_3$ aligned with the orbit normal direction: $\hat{\boldsymbol{b}}_3 = \hat{\boldsymbol{o}}_h$ (refer to Figure 2, which shows an analogous radial spin case). As the spacecraft spins about its orbit normal axis at a constant rate ω, the axis $\hat{\boldsymbol{b}}_3$ remains aligned with $\hat{\boldsymbol{o}}_h$, while the remaining Hill frame axes $\hat{\boldsymbol{o}}_r$ and $\hat{\boldsymbol{o}}_\theta$ rotate in the $\hat{\boldsymbol{b}}_1$–$\hat{\boldsymbol{b}}_2$ plane. The time-dependent rotation of the Hill frame with respect to the body frame can be described by a DCM, which is equivalent to a rotation about the $\hat{\boldsymbol{b}}_3$ axis:

$$[M_3(t)] = \begin{bmatrix} \cos(\omega t) & \sin(\omega t) & 0 \\ \text{-}\sin(\omega t) & \cos(\omega t) & 0 \\ 0 & 0 & 1 \end{bmatrix} \tag{6}$$

Substituting this rotation matrix into Equation (5) yields the position vector expressed in the body frame as:

$$^{B}\begin{bmatrix} x(t) \\ y(t) \\ z(t) \end{bmatrix} = \begin{bmatrix} \cos(\omega t)[A_0 \cos(nt + \beta) + x_{\text{off}}] + \sin(\omega t)[-2A_0 \sin(nt + \alpha) - \frac{3}{2} nt x_{\text{off}} + y_{\text{off}}] \\ - \sin(\omega t)[A_0 \cos(nt + \beta) + x_{\text{off}}] + \cos(\omega t)[-2A_0 \sin(nt + \alpha) - \frac{3}{2} nt x_{\text{off}} + y_{\text{off}}] \\ B_0 \cos(nt + \beta) \end{bmatrix} \tag{7}$$

As in the Hill frame, the out-of-plane motion (along the z-axis) remains decoupled from the in-plane dynamics and follows a simple harmonic oscillator, with amplitude B_0 and phase angle β. However, the in-plane motion is now modulated by the spin rate ω, introducing time-varying coupling between the radial and along-track components in the body frame. The resulting motion depends strongly on the relationship between the spin rate and the orbital mean motion. Different behaviors emerge depending on whether this relationship is resonant or non-resonant, which are explored in the following subsections.

Resonant spin

In the resonant spin case, the chief spacecraft spins at one revolution per orbit, such that the spin rate equals the orbital mean motion ($\omega = n$). Under this condition, the transformation of the relative motion into the body frame simplifies significantly, and the equation of motion becomes:

$$
{}^{B}\begin{bmatrix} x(t) \\ y(t) \\ z(t) \end{bmatrix} = \begin{bmatrix} (y_{\text{off}} - \frac{3}{2}ntx_{\text{off}})\sin(nt) + x_{\text{off}}\cos(nt) + \frac{3}{2}A_0\cos(2nt+\alpha) - \frac{1}{2}A_0\cos(\alpha) \\ (y_{\text{off}} - \frac{3}{2}ntx_{\text{off}})\cos(nt) - x_{\text{off}}\sin(nt) - \frac{3}{2}A_0\sin(2nt+\alpha) - \frac{1}{2}A_0\sin(\alpha) \\ B_0\cos(nt+\beta) \end{bmatrix} \tag{8}
$$

Using the following trigonometric identities:

$$
\begin{aligned}
A\sin x + B\cos x &= \sqrt{A^2+B^2}\cos\left(x - \tan^{-1}\left(\frac{A}{B}\right)\right) \\
A\sin x + B\cos x &= \sqrt{A^2+B^2}\sin\left(x - \tan^{-1}\left(\frac{B}{-A}\right)\right)
\end{aligned} \tag{9}
$$

the in-plane motion can be rewritten in a more geometrically intuitive form as:

$$
{}^{B}\begin{bmatrix} x(t) \\ y(t) \\ z(t) \end{bmatrix} = \begin{bmatrix} 2r\sin(nt-\phi) + d\cos(2nt-\gamma) - \frac{d}{3}\cos\alpha \\ 2r\cos(nt-\phi) - d\sin(2nt-\gamma) - \frac{d}{3}\sin\alpha \\ B_0\cos(nt+\beta) \end{bmatrix} \tag{10}
$$

where:

$$
\begin{aligned}
r &= \frac{1}{2}\sqrt{\left(y_{\text{off}} - \frac{3ntx_{\text{off}}}{2}\right)^2 + x_{\text{off}}^2} \qquad & \gamma &= -\alpha \\
d &= \frac{3A_0}{2} & \phi &= \tan^{-1}\left(\frac{-x_{\text{off}}}{y_{\text{off}} - \frac{3ntx_{\text{off}}}{2}}\right)
\end{aligned} \tag{11}
$$

The resulting trajectory in the $\hat{\boldsymbol{b}}_1$–$\hat{\boldsymbol{b}}_2$ plane forms an epitrochoid, the path traced by a point on a circle rolling around the outside of a fixed circle of the same radius as seen in Figure 4.

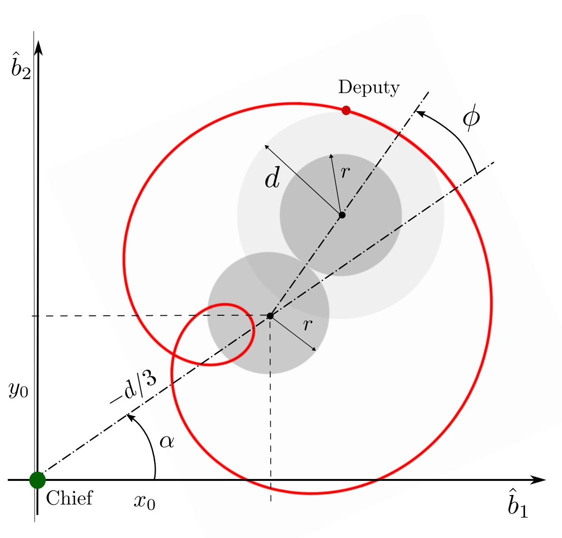

Figure 4. Epitrochoid parameters visualization

In this context, r is the radius of both the fixed and rolling circles, d is the arm length (distance from the tracing point to the center of the rolling circle), $-d/3$ is the offset of the fixed circle from the chief, α defines the orientation of the epitrochoid, ϕ is the phase offset of the rolling circle. These parameters form a new, intuitive set of body-frame orbital elements, analogous to the LROEs and IROEs, which provide a geometric interpretation of the motion in the rotating frame. In fact, for this specific case of resonant orbit normal spin, the resulting set of elements closely resembles those derived in the inertial frame,[22] with the radius r being identical in both formulations.

When there is no difference in semi-major axes between the chief and deputy ($x_{\text{off}} = 0$), the motion simplifies further. In this case, all epitrochoid parameters become time-invariant. The radius r depends solely on y_{off}, while the arm length d is only a function of A_0. The shape and size of the trajectory are fully decoupled from the orientation (α). These relationships are visualized in Figure 5, which also serves to validate the simplified body-frame equation of motion. The solid red curve represents the trajectory computed directly from Equation (8), while the dashed yellow curve shows the equivalent motion derived from the reformulated epitrochoid expression in Equation (10). The size of the relative orbit varies with r, while its shape depends on the ratio r/d. The orbit's offset is governed by d, and its orientation is controlled by the angular parameter α.

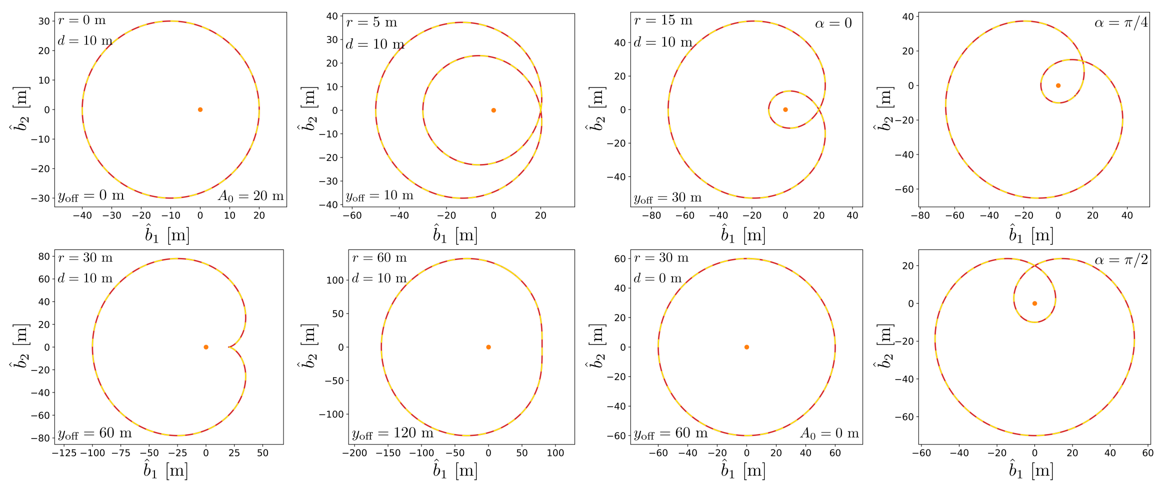

Figure 5. Bounded body-frame relative trajectory for a circular chief orbit with constant and resonant orbit-normal spin motion. The solid red line is generated from the initial equation, while the dashed yellow curve corresponds to the simplified epitrochoid equation.

Drift motion

When $x_{\text{off}} \neq 0$, two key parameters of the epitrochoid, namely the radius r and the phase angle ϕ, become time-dependent. This time variation introduces a gradual drift in the relative trajectory within the body frame, as the size of the orbit evolve over time. The result is a shifting epitrochoid pattern that no longer traces a closed curve. Instead, the trajectory exhibits a spiraling motion, either expanding away from or converging toward the chief spacecraft, depending on the sign of x_{off}. This behavior is illustrated in Figure 6. In the right subplot, the inward drift corresponds to a deputy spacecraft gradually approaching the chief, while in the left one, a negative offset causes the relative motion to spiral outward.

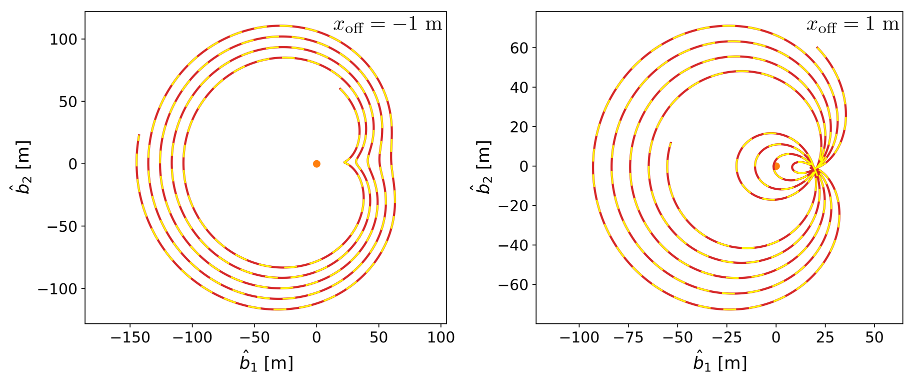

Figure 6. Unbounded body-frame relative trajectory for a circular chief orbit with constant and resonant orbit-normal spin motion. The solid red line is generated from the initial equation, while the dashed yellow curve corresponds to the simplified epitrochoid equation.

Non-resonant spin

When the chief spacecraft's spin rate is not equal to the orbital mean motion, $\omega \neq n$, the relative motion described in Equation (7) becomes less intuitive. However, certain simplifications can still be made for special cases.

One such case arises when there is no initial offset in the Hill frame in either the radial or along-track directions, meaning $x_{\text{off}} = y_{\text{off}} = 0$. Under this condition, the body-frame equation of motion simplifies to:

$$^{B}\begin{bmatrix} x(t) \\ y(t) \\ z(t) \end{bmatrix} = \begin{bmatrix} -\frac{1}{2}A_0 \cos\left((n-\omega)t+\alpha\right) + \frac{3}{2}A_0 \cos\left((n+\omega)t+\alpha\right) \\ -\frac{1}{2}A_0 \sin\left((n-\omega)t+\alpha\right) - \frac{3}{2}A_0 \sin\left((n+\omega)t+\alpha\right) \\ B_0 \cos(nt+\beta) \end{bmatrix} \tag{12}$$

The nature of the in-plane motion depends on the relative magnitudes of n and ω. Two distinct geometric interpretations emerge:

Case 1: Spin Rate Lower than Orbit Rate ($\omega < n$)

In this case, the motion corresponds to a hypotrochoid, a curve traced by a point on a circle rolling inside a larger fixed circle (see Figure 7). The trajectory can be described using the following parametric form:

$$^{B}\begin{bmatrix} x(t) \\ y(t) \end{bmatrix} = \begin{bmatrix} d\cos\left(\frac{R-r}{r}\theta - \phi\right) - (R-r)\cos(\theta-\phi) \\ -d\sin\left(\frac{R-r}{r}\theta - \phi\right) - (R-r)\sin(\theta-\phi) \end{bmatrix} \tag{13}$$

where:

$$\begin{aligned} R &= A_0 \frac{n}{n+\omega} & \theta &= (n-\omega)t \\ r &= \frac{A_0}{2} \cdot \frac{n-\omega}{n+\omega} & \phi &= -\alpha \\ d &= \frac{3}{2}A_0 \end{aligned} \tag{14}$$

Here, R is the radius of the fixed (outer) circle centered at the chief, r is the radius of the rolling (inner) circle, and d is the arm length, the distance from the tracing point to the center of the rolling circle. The rotation of the curve in the $\hat{\boldsymbol{b}}_1$–$\hat{\boldsymbol{b}}_2$ plane about the $\hat{\boldsymbol{b}}_3$ axis is governed by the angle α.

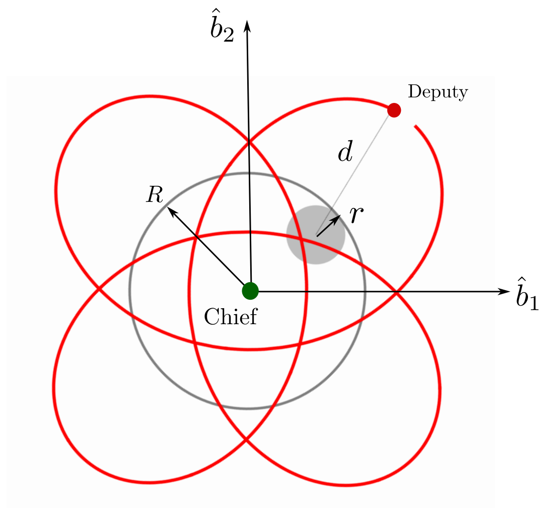

Figure 7. Hypotrochoid parameters visualization

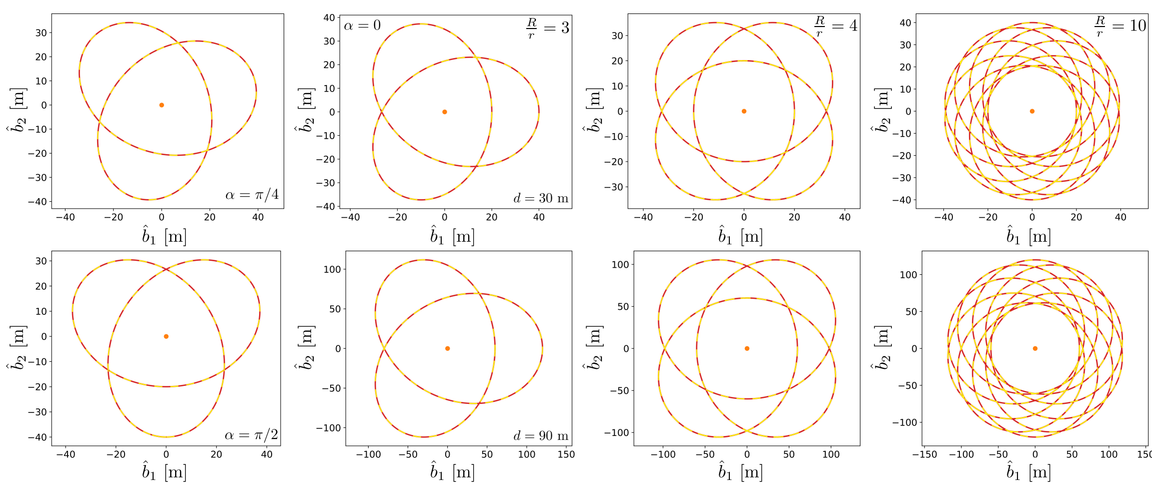

Figure 8. Bounded body-frame relative trajectory for a circular chief orbit with orbit-normal spin motion, where orbit rate is greater than spin rate. The solid red line is generated from the initial equation, while the dashed yellow curve corresponds to the simplified hyptrochoid equation.

Figure 8 shows the resulting in-plane relative motion in the body frame for this non-resonant spin case. The solid red line represents the trajectory computed from Equation (7), while the dashed yellow curve shows the corresponding results from the parametric form. As expected, the motion traces a closed hypotrochoidal path. The overall size of the trajectory is governed by the arm length d, which depends on the LROEs amplitude parameter A_0. The shape of the curve is determined by the ratio $\frac{R}{r} = \frac{2n}{n-\omega}$, which is set by the spin-to-orbit frequency ratio and is always greater than 2 in this case. The orientation of the curve is defined by the parameter α.

Case 2: Spin Rate Greater than Orbit Rate ($\omega > n$)

When the spin rate exceeds the orbit rate, the simplified equation of motion becomes:

$$ {}^{B}\begin{bmatrix} x(t) \\ y(t) \end{bmatrix} = \begin{bmatrix} -\frac{1}{2}A_0 \cos\left((\omega - n)t - \alpha\right) + \frac{3}{2}A_0 \cos\left((n+\omega)t + \alpha\right) \\ \frac{1}{2}A_0 \sin\left((\omega - n)t - \alpha\right) - \frac{3}{2}A_0 \sin\left((n+\omega)t + \alpha\right) \end{bmatrix} \tag{15} $$

The motion corresponds to an epitrochoid and can be expressed in the following parametric form:

$$ {}^{B}\begin{bmatrix} x(t) \\ y(t) \end{bmatrix} = \begin{bmatrix} d\cos\left(\frac{R+r}{r}\theta - \phi\right) - (R+r)\cos(\theta + \phi) \\ -d\sin\left(\frac{R+r}{r}\theta - \phi\right) + (R+r)\sin(\theta + \phi) \end{bmatrix} \tag{16} $$

where:

$$ \begin{aligned} R &= A_0 \frac{n}{n+\omega} \qquad & \theta &= (\omega - n)t \\ r &= \frac{1}{2}A_0 \frac{\omega - n}{n+\omega} \qquad & \phi &= \alpha \\ d &= \frac{3}{2}A_0 \end{aligned} \tag{17} $$

In this configuration, the two circles have unequal radii: R is the radius of the fixed (inner) circle centered at the chief, r is the radius of the rolling (outer) circle, and d is the arm length. The shape of the curve depends on the ratio $\frac{R}{r} = \frac{2n}{\omega-n}$, which depends on the relative spin and orbit rates. The overall size of the motion is a function of the arm length d, which is again controlled by the amplitude parameter A_0, as in the previous case. The orientation of the curve is determined by the angular parameter α. The figure below shows different trajectory shapes for different ratios and compares the trajectory obtained from the simplified epitrochoid form (dashed yellow line) with the one computed from the original full dynamics (solid red line) using Equation (7). The agreement confirms the validity of the simplified model.

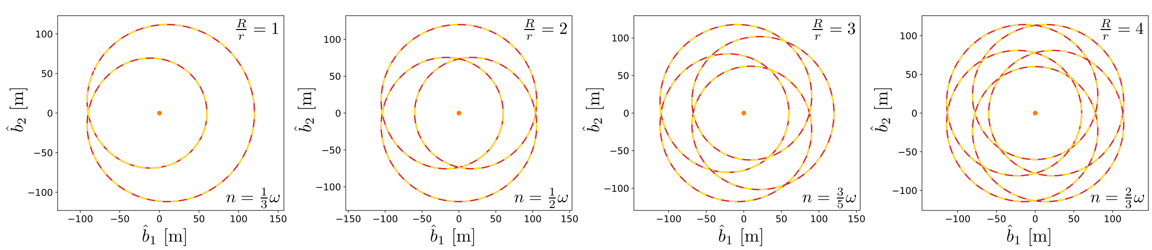

Figure 9. Bounded body-frame relative trajectory for a circular chief orbit with orbit-normal spin motion, where spin rate is greater than orbit rate. The solid red line is generated from the initial equation, while the dashed yellow curve corresponds to the simplified epitrochoid equation.

The first plot corresponds to a special case in which the radii of the fixed and rolling circles are equal, as in the resonant condition (Figure 4). This leads to a simpler closed curve known as a Limaçon.

NADIR SPIN

The second case examined in this study involves a constant-rate spin about the radial (nadir-pointing) direction, denoted by $\hat{\boldsymbol{o}}_r$. In all scenarios, the body frame is initially aligned with the Hill frame such that $\hat{\boldsymbol{b}}_1 = \hat{\boldsymbol{o}}_r$ at time $t = 0$ (see Figure 2). In this configuration, since the Hill frame itself is rotating, the system exhibits a dual-spin behavior compared to an inertial frame: the body frame both follows the rotation of the Hill frame to maintain radial alignment and simultaneously spins at a constant rate about the radial axis. As a result, $\hat{\boldsymbol{b}}_1$ remains aligned with $\hat{\boldsymbol{o}}_r$ over time, while the along-track and cross-track axes, $\hat{\boldsymbol{o}}_\theta$ and $\hat{\boldsymbol{o}}_h$, rotate within the plane orthogonal to the spin axis. The DCM $[BH]$, which maps vectors from the Hill frame to the body frame, is thus a time-dependent rotation matrix given by:

$$[BH] = [M_1(t)] = \begin{bmatrix} 1 & 0 & 0 \\ 0 & \cos(\omega t) & -\sin(\omega t) \\ 0 & \sin(\omega t) & \cos(\omega t) \end{bmatrix} \tag{18}$$

Applying this DCM to Equation (5) yields the expression for the relative motion in the body frame:

$$^{B}\begin{bmatrix} x(t) \\ y(t) \\ z(t) \end{bmatrix} = \begin{bmatrix} A_0 \cos(nt+\alpha) + x_{\text{off}} \\ B_0 \cos(nt+\beta)\sin(\omega t) + \cos(\omega t)[-2A_0 \sin(nt+\alpha) - \frac{3}{2}ntx_{\text{off}} + y_{\text{off}}] \\ B_0 \cos(nt+\beta)\cos(\omega t) + \sin(\omega t)[2A_0 \sin(nt+\alpha) + \frac{3}{2}ntx_{\text{off}} - y_{\text{off}}] \end{bmatrix} \tag{19}$$

Resonant spin with bounded Motion

In the special case of bounded motion ($x_{\text{off}} = 0$) and resonant spin rate ($\omega = n$), the expression simplifies considerably:

$$^{B}\begin{bmatrix} x(t) \\ y(t) \\ z(t) \end{bmatrix} = \begin{bmatrix} A_0 \cos(nt+\alpha) \\ y_{\text{off}}\cos(nt) - A_0\sin(2nt+\alpha) - \frac{B_0}{2}\sin(2nt+\beta) - A_0\sin(\alpha) + \frac{B_0}{2}\sin(\beta) \\ y_{\text{off}}\sin(nt) + A_0\cos(2nt+\alpha) + \frac{B_0}{2}\cos(2nt+\beta) - A_0\cos(\alpha) + \frac{B_0}{2}\cos(\beta) \end{bmatrix} \tag{20}$$

The motion along the x-axis is simply a harmonic oscillation with the element A_0 defining its amplitude, and the angular element α defining its phase. However, unlike the previous case, the motion is now coupled across all three axes. Using the trigonometric identities below and those in Equation (9), the expression for the y and z components can be further simplified:

$$\begin{aligned} A\cos x + B\cos y &= (A+B)\cos\left(\frac{x-y}{2}\right)\cos\left(\frac{x+y}{2}\right) + (B-A)\sin\left(\frac{x-y}{2}\right)\sin\left(\frac{x+y}{2}\right) \\ A\sin x + B\sin y &= (A+B)\cos\left(\frac{x-y}{2}\right)\sin\left(\frac{x+y}{2}\right) + (A-B)\sin\left(\frac{x-y}{2}\right)\cos\left(\frac{x+y}{2}\right) \end{aligned} \tag{21}$$

resulting in the compact form:

$$^{B}\begin{bmatrix} x(t) \\ y(t) \\ z(t) \end{bmatrix} = \begin{bmatrix} A_0\cos(nt+\alpha) \\ 2r\cos(nt) - d\sin(2nt-\gamma) + y_0 \\ -2r\sin(nt) - d\cos(2nt-\gamma) + z_0 \end{bmatrix} \tag{22}$$

where the parameters are defined as:

$$
\begin{aligned}
r &= \frac{1}{2} y_{\text{off}} \\
d &= \sqrt{A_0^2 + \frac{B_0^2}{4} - A_0 B_0 \cos(\alpha - \beta)} \\
\gamma &= -\frac{\alpha + \beta}{2} + \tan^{-1}\left(-\frac{2A_0 + B_0}{2A_0 - B_0} \tan\left(\frac{\alpha - \beta}{2}\right)\right) \\
y_0 &= -A_0 \sin\alpha - \frac{B_0}{2} \sin\beta \\
z_0 &= A_0 \cos\alpha + \frac{B_0}{2} \cos\beta
\end{aligned}
\tag{23}
$$

For the special case where $B_0 = 2A_0$, the expressions for d and γ simplify to:

$$
\begin{aligned}
d &= 2A_0 \sin\left(\frac{\alpha - \beta}{2}\right) \\
\gamma &= -\frac{\alpha + \beta}{2}
\end{aligned}
\tag{24}
$$

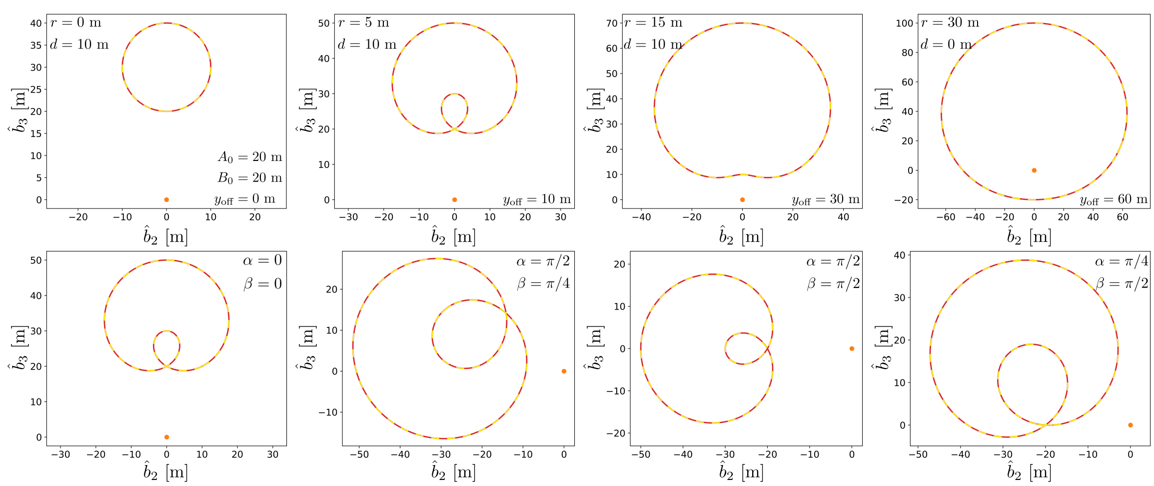

Figure 10. Bounded body-frame relative trajectory for a circular chief orbit with constant and resonant nadir spin motion. The solid red line is generated from the initial equation, while the dashed yellow curve corresponds to the simplified epitrochoid equation.

The trajectory in the $\hat{\boldsymbol{b}}_2$–$\hat{\boldsymbol{b}}_3$ plane corresponds to an epitrochoid. Unlike the previous case, the offset here is not constant, but represented by the coupled cartesian components y_0 and z_0. These parameters in (23) and (24) provide a new set of body-frame orbital elements tailored to the resonant nadir spin configuration. To validate the simplified expression in Equation (22), Figure 10 compares the body-frame trajectory obtained directly from Equation (19) (solid red) against the simplified form (dashed yellow), confirming their agreement. The size of the relative orbit varies with r, which is only a function of y_{off}, as shown in the first line of plots. The shape of the trajectory depends on the ratio r/d. The arm length d, along with the offset and orientation of the curve, are all coupled and influenced by A_0, B_0, α, and β.

Unbounded motion

Introducing a nonzero drift term ($x_{\text{off}} \neq 0$) affects only the radius r, making it time-dependent:

$$r = \frac{1}{2}\left(y_{\text{off}} - \frac{3}{2}ntx_{\text{off}}\right) \tag{25}$$

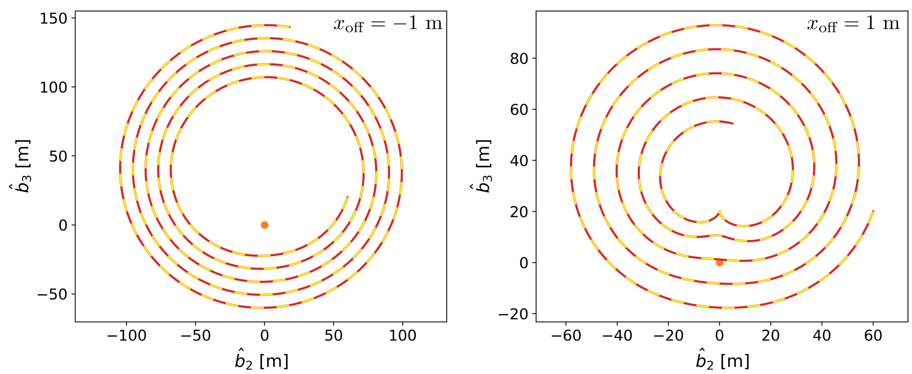

Figure 11. Unbounded body-frame relative trajectory for a circular chief orbit with constant and resonant nadir spin motion. The solid red line is generated from the initial equation, while the dashed yellow curve corresponds to the simplified epitrochoid equation.

As in the Hill frame and previous spin case, this produces unbounded relative motion in the form of a drifting epitrochoid. Depending on the sign of x_{off}, the orbit either expands or contracts over time, approaching or diverging from the chief, as illustrated in Figure 11.

Non resonant case

The non-resonant case is more complex to express in an intuitive geometric form. While the resulting motion still resembles trochoidal curves, many parameters become time-varying, which reduces the clarity of the geometric interpretation. However, in the special case where the phase angles vanish ($\alpha = \beta = 0$) and no drift is present ($x_{\text{off}} = 0$), the trajectory equations simplify to:

$$^{B}\begin{bmatrix} x(t) \\ y(t) \\ z(t) \end{bmatrix} = \begin{bmatrix} A_0 \cos(nt + \alpha) \\ y_{\text{off}} \cos(\omega t) - \left(A_0 - \frac{B_0}{2}\right) \sin\left((n+\omega)t\right) - \left(A_0 + \frac{B_0}{2}\right) \sin\left((n-\omega)t\right) \\ -y_{\text{off}} \sin(\omega t) - \left(A_0 - \frac{B_0}{2}\right) \cos\left((n+\omega)t\right) + \left(A_0 + \frac{B_0}{2}\right) \cos\left((n-\omega)t\right) \end{bmatrix} \tag{26}$$

Despite the remaining time-varying components, certain special cases allow a reformulation in terms of geometric invariants, yielding more insight into the motion characteristics. These cases are discussed below.

Case 1: $2A_0 = B_0$

In this case, the second term in the y and z component of Equation (26) cancel, leading to the following equation:

$$
{}^{B}\begin{bmatrix} x(t) \\ y(t) \\ z(t) \end{bmatrix} = \begin{bmatrix} A_0 \cos(nt + \alpha) \\ y_{\text{off}} \cos(\omega t) - 2A_0 \sin\left((n - \omega)t\right) \\ -y_{\text{off}} \sin(\omega t) + 2A_0 \cos\left((n - \omega)t\right) \end{bmatrix} \tag{27}
$$

Depending on the relationship between the orbit rate n and spin rate ω, this motion can be interpreted as either a hypotrochoid or an epitrochoid.

Case 1.1: Orbit Rate Greater than Spin Rate $(n > \omega)$

The motion in the $\hat{\boldsymbol{b}}_2$-$\hat{\boldsymbol{b}}_3$-plane can be described by a hypotrochoid with the following parametric form:

$$
{}^{B}\begin{bmatrix} x(t) \\ y(t) \\ z(t) \end{bmatrix} = \begin{bmatrix} A_0 \cos(nt) \\ (R - r) \cos(\omega t) - d \sin\left(\frac{R-r}{r} \omega t\right) \\ -(R - r) \sin(\omega t) + d \cos\left(\frac{R-r}{r} \omega t\right) \end{bmatrix} \tag{28}
$$

with:

$$
\begin{aligned} r &= \frac{\omega}{n - \omega} y_{\text{off}} \\ R &= \frac{n}{n - \omega} y_{\text{off}} \\ d &= 2A_0 = B_0 \end{aligned} \tag{29}
$$

This matches the qualitative behavior shown in Figure 8, where the shape is governed by the ratio $R/r = n/\omega$, and the overall size scales with B_0, or A_0.

Case 1.2: Spin Rate Greater than Orbit Rate $(\omega > n)$

When the spin rate exceeds the orbit rate, Equation (27) transforms into:

$$
{}^{B}\begin{bmatrix} x(t) \\ y(t) \\ z(t) \end{bmatrix} = \begin{bmatrix} A_0 \cos(nt + \alpha) \\ y_{\text{off}} \cos(\omega t) + 2A_0 \sin\left((\omega - n)t\right) \\ -y_{\text{off}} \sin(\omega t) + 2A_0 \cos\left((\omega - n)t\right) \end{bmatrix} \tag{30}
$$

which can be formulated as a parametric equation of an epitrochoid:

$$
{}^{B}\begin{bmatrix} x(t) \\ y(t) \\ z(t) \end{bmatrix} = \begin{bmatrix} A_0 \cos(nt) \\ (R + r) \cos(\omega t) + d \sin\left(\frac{R+r}{r} \omega t\right) \\ (R + r) \sin(\omega t) - d \cos\left(\frac{R+r}{r} \omega t\right) \end{bmatrix} \tag{31}
$$

with:

$$
\begin{aligned} r &= \frac{\omega - n}{\omega} B_0 = 2\frac{\omega - n}{\omega} A_0 \\ R &= \frac{n}{\omega} B_0 = 2\frac{n}{\omega} A_0 \\ d &= y_{\text{off}} \end{aligned} \tag{32}
$$

This behavior corresponds to that shown in Figure 9, where the shape depends on the ratio R/r, related to the relative difference between n and ω. The overall scale of the orbit is influenced primarily by y_{off}, which acts as the arm length.

Case 2: Planar motion in the Hill frame ($B_0 = 0$)

An interesting special case occurs when the spacecraft's motion in the Hill frame is planar, meaning $B_0 = 0$. The resulting trajectory in the $\hat{\boldsymbol{b}}_2$-$\hat{\boldsymbol{b}}_3$-plane describes a hypotrochoid with a time-varying arm length:

$$^{B}\begin{bmatrix} x(t) \\ y(t) \\ z(t) \end{bmatrix} = \begin{bmatrix} A_0 \cos(nt) \\ (R-r)\cos(\omega t) - d\cos\left(\frac{R-r}{r}\omega t\right) \\ -(R-r)\sin(\omega t) + d\sin\left(\frac{R-r}{r}\omega t\right) \end{bmatrix} \tag{33}$$

with:

$$\begin{aligned} r &= y_{\text{off}} \\ R &= 2y_{\text{off}} \\ d &= 2A_0\sin(nt) \end{aligned} \tag{34}$$

This produces a shape similar to that shown in Figure 3(a), where the arm length varies periodically over time. An example is shown in Figure 12.

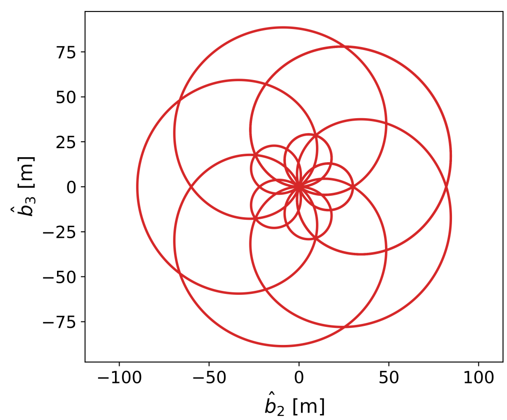

Figure 12. Body-frame relative trajectory for a circular chief orbit with constant, non-resonant nadir spin. The relative motion in the Hill frame is planar, resulting in a bounded, time-varying trochoidal pattern in the body frame.

The arm length oscillates sinusoidally with an amplitude of $2A_0$. Over time, this leads to a shape resembling the superposition of two hypotrochoids of different scales. Figure 13 presents the trajectory over one orbital period. In this case the ratio $R/r = 2$ remains constant, while both R and r are proportional to y_{off}. This parameter slightly affects the shape, as illustrated in the differences between the top and bottom rows of plots in Figure 13. More significant shape changes arise from the ratio ω/n, which alters the relative proportions of the arm length and base circle radius (compare across columns in the figure). Changing the parameter A_0 scales the trajectory without altering its shape, as it only modifies the amplitude of the arm length oscillation.

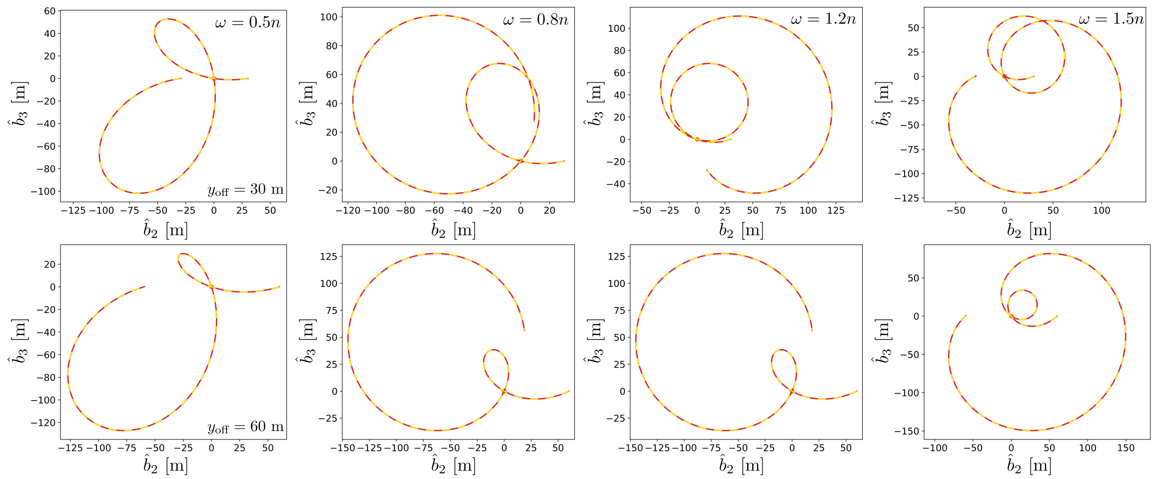

Figure 13. Body-frame relative trajectory for a circular chief orbit with constant, non-resonant nadir spin. The relative motion in the Hill frame is planar, leading to a time-varying trochoidal pattern in the body frame. The solid red line is generated from the initial equation, while the dashed yellow curve corresponds to the simplified hypotrochoid equation.

A similar result is obtained when the spacecraft exhibits purely out-of-plane motion in the Hill frame ($A_0 = 0$ and $B_0 \neq 0$). In that case, the motion is entirely in the $\hat{\boldsymbol{b}}_2$-$\hat{\boldsymbol{b}}_3$-plane ($x(t) = 0$), and the arm length becomes:

$$d = B_0 \sin(nt) \tag{35}$$

ALONG TRACK SPIN

For completeness, the case is examined where the spacecraft spins at a constant rate about the along-track direction, which aligns with the velocity vector. As with the previous configurations, since the Hill frame itself is rotating, this setup results in a dual-spin motion relative to the inertial frame: the body maintains alignment with the along-track direction while simultaneously spinning about it. The DCM mapping from the Hill frame to the body frame in this case:

$$[M_2(t)] = \begin{bmatrix} \cos(\omega t) & 0 & \sin(\omega t) \\ 0 & 1 & 0 \\ \text{-}\sin(\omega t) & 0 & \cos(\omega t) \end{bmatrix} \tag{36}$$

Substituting this into Equation (5), the body-frame expression for the relative motion becomes:

$$^{B}\begin{bmatrix} x(t) \\ y(t) \\ z(t) \end{bmatrix} = \begin{bmatrix} A_0 \cos(nt+\alpha)\cos(\omega t) + B_0 \cos(nt+\beta)\sin(\omega t) \\ -2A_0 \sin(nt+\alpha) - \frac{3}{2} nt x_{\text{off}} + y_{\text{off}} \\ B_0 \cos(nt+\beta)\cos(\omega t) - \sin(\omega t)[A_0 \cos(nt+\alpha) + x_{\text{off}}] \end{bmatrix} \tag{37}$$

In this configuration, a drift term appears only along the along-track direction (the $\hat{\boldsymbol{b}}_2$-axis). The motion in this direction is a coupled harmonic oscillation with amplitude $2A_0$, phase angle α, and constant offset y_{off}. When $x_{\text{off}} \neq 0$, a linear drift is introduced. However, this drift affects only the along-track component; the motion in the $\hat{\boldsymbol{b}}_1$-$\hat{\boldsymbol{b}}_3$-plane remains bounded and can have the following shapes:

- When $x_{\text{off}} = 0$, the trajectory in the $\hat{\boldsymbol{b}}_1$-$\hat{\boldsymbol{b}}_3$-plane forms a circular path, with the radius R defining its size, and the offset of its center from the chief is given by the two Cartesian components x_0 and z_0. ϕ is the phase angle. The parameters are all coupled and defined as follows:

$$\begin{aligned} R &= \frac{1}{2}\sqrt{A_0^2 + B_0^2 - 2A_0B_0\sin(\alpha-\beta)} & x_0 &= \frac{A_0}{2}\cos\alpha + \frac{B_0}{2}\sin\beta \\ \phi &= \tan^{-1}\left(\frac{B_0\sin\beta + A_0\cos\alpha}{A_0\sin\alpha - B_0\cos\beta}\right) & z_0 &= \frac{A_0}{2}\sin\alpha + \frac{B_0}{2}\cos\beta \end{aligned} \tag{38}$$

- When $x_{\text{off}} \neq 0$, the trajectory becomes an epitrochoid, defined by the parameter given in Equation (39). The obtained trajectory shapes for this case are very similar to those given in Figure 10: The center of the epitrochoid does not have a constant offset from the chief, but it is instead defined by the Cartesian components x_0 and z_0. The offset, the phase angle ϕ, and the arm length d are all coupled and a function of A_0, B_0, α, and β. The only decoupled parameter is the radius r, that determines the size of the trajectory, and is only a function of x_{off}. The shape of the relative orbit depend on the ratio of r/d.

$$\begin{aligned} r &= x_{\text{off}}/2 & x_0 &= \frac{A_0}{2}\cos\alpha + \frac{B_0}{2}\sin\beta \\ \phi &= \tan^{-1}\left(\frac{B_0\sin\beta + A_0\cos\alpha}{A_0\sin\alpha - B_0\cos\beta}\right) & z_0 &= \frac{A_0}{2}\sin\alpha + \frac{B_0}{2}\cos\beta \\ d &= \frac{1}{2}\sqrt{A_0^2 + B_0^2 - 2A_0B_0\sin(\alpha-\beta)} \end{aligned} \tag{39}$$

- In the non-resonant case with: $\alpha = \beta = 0$ and $x_{\text{off}} = 0$:
  - When the orbital rate exceeds the spin rate ($n > \omega$), the resulting trajectory traces a hypotrochoid. In this case, R is the radius of the fixed circle centered at the chief, r is the radius of the rolling circle, and d is the arm length from the center of the rolling circle to the tracing point. The overall size of the trajectory is governed by the arm length d, while its shape is determined by the ratio R/r, which is directly related to the ratio n/ω. The orientation of the curve is influenced by the angles ϕ, and γ. However, all hypotrochoid parameters, R, r, d, ϕ, and γ, are interdependent and functions of the LROEs A_0 and B_0. The resulting shapes resemble those shown in Figure 8.

$$\begin{aligned} R &= \frac{n}{n+\omega}\sqrt{A_0^2 + B_0^2} & \gamma &= \tan^{-1}\left(\frac{B_0}{A_0}\right) \\ r &= \frac{1}{2}\cdot\frac{n-\omega}{n+\omega}\sqrt{A_0^2 + B_0^2} & \phi &= \tan^{-1}\left(\frac{A_0}{B_0}\right) \\ d &= \frac{1}{2}\sqrt{A_0^2 + B_0^2} \end{aligned} \tag{40}$$

    The equation of motion in the $\hat{\boldsymbol{b}}_1$-$\hat{\boldsymbol{b}}_3$-plane is given by:

$${}^{B}\begin{bmatrix} x(t) \\ z(t) \end{bmatrix} = \begin{bmatrix} d\sin\left(\frac{R-r}{r}(n-\omega)t - \gamma\right) + (R-r)\cos\left((n-\omega)t - \phi\right) \\ d\cos\left(\frac{R-r}{r}(n-\omega)t - \gamma\right) + (R-r)\sin\left((n-\omega)t - \phi\right)] \end{bmatrix} \tag{41}$$

– When the spin rate exceeds the orbital rate ($n < \omega$), the resulting trajectory forms an epitrochoid, with shapes similar to those illustrated in Figure 9. The parameters defining this motion are given by:

$$\begin{aligned} R &= \frac{n}{n+\omega}\sqrt{A_0^2+B_0^2} & d &= \frac{1}{2}\sqrt{A_0^2+B_0^2} \\ r &= \frac{1}{2}\cdot\frac{\omega-n}{n+\omega}\sqrt{A_0^2+B_0^2} & \phi &= \tan^{-1}\left(-\frac{A_0}{B_0}\right) \end{aligned} \tag{42}$$

Here, d represents the arm length and determines the overall size of the trajectory. The radius of the fixed circle centered at the chief is denoted by R, while r is the radius of the rolling circle. The shape of the trajectory is governed by the ratio R/r, which is directly related to the ratio n/ω. The orientation of the epitrochoid in the plane is determined by the phase angle ϕ. The motion in the $\hat{\boldsymbol{b}}_1$–$\hat{\boldsymbol{b}}_3$ plane is described by the following equation:

$$^{B}\begin{bmatrix} x(t) \\ z(t) \end{bmatrix} = \begin{bmatrix} d\cos\left(\frac{R+r}{r}(n-\omega)t-\phi\right)+(R+r)\cos\left((\omega-n)t-\phi\right) \\ d\cos\left(\frac{R-r}{r}(n-\omega)t-\phi\right)+(R+r)\sin\left((\omega-n)t-\phi\right)] \end{bmatrix} \tag{43}$$

CONCLUSION

This work investigates relative motion trajectories observed from the body frame of a spinning chief spacecraft. While prior studies focused on inertially fixed (non-rotating) configurations, this paper extends the analysis to spinning chiefs, specifically those rotating at a constant rate about a principal body axis initially aligned with the Hill frame. Three orientations are considered: orbit-normal, radial, and along-track. The analysis uses closed-form Clohessy-Wiltshire (CW) equations, limiting applicability to circular chief orbits. These scenarios are more likely to occur in controlled or operational spacecraft, rather than in non-cooperative targets. Among them, the orbit-normal spin configuration is particularly relevant for missions involving a chief that requires continuous Earth- or nadir-pointing.

Both resonant (spin rate equals orbital rate) and non-resonant cases are explored, including the effect of semi-major axis offsets, which typically cause body-frame drift of otherwise bounded motion, mirroring Hill frame behavior. Analytical derivations and geometric interpretations reveal that under certain conditions, such as resonance or specific Hill frame motions, relative trajectories in the body frame form closed, regular patterns (e.g., circles, epitrochoids, hypotrochoids). These cases allow the use of time-invariant geometric parameters, analogous to LROEs and IROEs, to compactly describe the dynamics. In more general configurations, however, these parameters become time-varying and lose their geometric clarity. The main contribution of this work lies in identifying and formalizing the special cases where body-frame motion can be described with geometrically insightful, time-invariant parameters. New parameter sets are introduced to characterize the deputy's trajectory shape and location for each case. These descriptions offer more intuitive information about the deputy's proximity to key body axes, its direction of motion, and its potential to remain in, drift toward, or avoid certain regions around the chief. Such insight is particularly useful for planning inspection, servicing, or docking maneuvers.

REFERENCES

[1] NASA Manned Spacecraft Center, "Gemini VII Mission Report," Tech. Rep. MSC-00171, NASA, Houston, Texas, 1966.

[2] M. D. Lallo, "Experience with the Hubble Space Telescope: 20 years of an archetype," *Optical Engineering*, Vol. 51, No. 1, 2012, pp. 011011–011011.

[3] NASA Satellite Servicing Projects Division, "NASA Satellite Servicing Projects Division: 2023 Project Report," tech. rep., NASA, Greenbelt, Maryland, 2023.

[4] G. Roesler, "Robotic Servicing of Geosynchronous Satellites (RSGS) Proposers Day," tech. rep., DARPA, 2016.

[5] R. B. Friend, "Orbital express program summary and mission overview," *Sensors and Systems for space applications II*, Vol. 6958, SPIE, 2008, pp. 11–21.

[6] C. Blackerby, A. Okamoto, S. Iizuka, Y. Kobayashi, K. Fujimoto, Y. Seto, S. Fujita, T. Iwai, N. Okada, J. Forshaw, *et al.*, "The ELSA-d end-of-life debris removal mission: preparing for launch," *Proceedings of the International Astronautical Congress, IAC*, Vol. 8, 2019.

[7] E. D. Wise, C. M. Pong, D. Miller, K. Cahoy, and T. T. Nguyen, "A dual-spinning, three-axis-stabilized cubesat for earth observations," *AIAA Guidance, Navigation, and Control (GNC) Conference*, 2013, p. 4716.

[8] D. McComas, F. Allegrini, P. Bochsler, M. Bzowski, M. Collier, H. Fahr, H. Fichtner, P. Frisch, H. Funsten, S. Fuselier, *et al.*, "The interstellar boundary explorer (IBEX)," *AIP Conference proceedings*, Vol. 719, American Institute of Physics, 2004, pp. 162–181.

[9] D. McComas, E. R. Christian, N. A. Schwadron, N. Fox, J. Westlake, F. Allegrini, D. Baker, D. Biesecker, M. Bzowski, G. Clark, *et al.*, "Interstellar mapping and acceleration probe (IMAP): A new NASA mission," *Space science reviews*, Vol. 214, No. 8, 2018, p. 116.

[10] S. Stoneman and R. Lampariello, "A Nonlinear Optimization Method to Provide Real-Time Feasible Reference Trajectories to Approach a Tumbling Target Satellite," *The International Symposium on Artificial Intelligence, Robotics and Automation in Space*, 06 2016.

[11] B.-Z. Zhou, X. Liu, and G.-P. Cai, "Motion-Planning and Pose-Tracking Based Rendezvous and Docking with a Tumbling Target," *Advances in Space Research*, Vol. 65, 11 2019, pp. 1139–1157, 10.1016/j.asr.2019.11.013.

[12] K. Albee, C. Oestreich, C. Specht, A. Terán Espinoza, J. Todd, I. Hokaj, R. Lampariello, and R. Linares, "A robust observation, planning, and control pipeline for autonomous rendezvous with tumbling targets," *Frontiers in Robotics and AI*, Vol. 8, 2021, p. 641338.

[13] J. Ventura, M. Ciarcia, M. Romano, and U. Walter, "An inverse dynamics-based trajectory planner for autonomous docking to a tumbling target," *AIAA guidance, navigation, and control conference*, 2016, p. 0876, 10.2514/6.2016-0876.

[14] G. Boyarko, O. Yakimenko, and M. Romano, "Optimal rendezvous trajectories of a controlled spacecraft and a tumbling object," *Journal of Guidance, Control, and dynamics*, Vol. 34, No. 4, 2011, pp. 1239–1252, 10.2514/1.47645.

[15] A. Fejzi and D. Miller, "Development of Control and Autonomy Algorithms for Autonomous Docking to Complex Tumbling Satellites," 2008.

[16] G. W. Hill, "Researches in the lunar theory," *American journal of Mathematics*, Vol. 1, No. 1, 1878, pp. 5–26, 10.2307/2369430.

[17] S. G. J. Sullivan and S. D'Amico, "Comprehensive Survey and Assessment of Spacecraft Relative Motion Dynamics Models," *Journal of Guidance, Control, and Dynamics*, Vol. 40, No. 8, 2017, p. 1837–1859, 10.2514/1.G002309.

[18] W. Clohessy and R. Wiltshire, "Terminal guidance system for satellite rendezvous," *Journal of the aerospace sciences*, Vol. 27, No. 9, 1960, pp. 653–658, 10.2514/8.8704.

[19] H. Schaub and J. L. Junkins, *Analytical mechanics of space systems*. AIAA, 4th ed., 2018, 10.2514/4.105210.

[20] H. Schaub, "Relative Orbit Geometry Through Classical Orbit Element Differences," *Journal of Guidance, Control and Dynamics*, Vol. 27, Sept.–Oct. 2004, pp. 839–848, 10.2514/1.12595.

[21] A. W. Koenig, T. Guffanti, and S. D'Amico, "New state transition matrices for relative motion of spacecraft formations in perturbed orbits," *AIAA/AAS astrodynamics specialist conference*, 2016, p. 5635, 10.2514/6.2016-5635.

[22] J. Hammerl and H. Schaub, "Orbiting Spacecraft Relative Motion In The Inertial Frame For Inertially Fixed Constraintsh," *AAS Spaceflight Mechanics Meeting*, Kauai, Hawaii, Jan. 19–23 2025. Paper No. AAS 25-207.